You can view the Version of Record for this article at: https://doi.org/10.1016/j.elstat.2018.02.001

A simplified formulation of wire-plate corona discharge in air: application to the ion wind simulation

M R Bouazza[1], K Yanallah[1], F Pontiga[2] and J H Chen[3]

[1]Laboratoire de Génie Electrique et des Plasmas, Université de Tiaret, Algeria
[2]Departamento de Física Aplicada II, Universidad de Sevilla, Spain
[3]Department of Mechanical Engineering, University of Wisconsin-Milwaukee, Milwaukee, WI 53211, USA

Abstract.

The spatial distribution of charged particles (electrons, negative ions and positive ions) and electric field have been evaluated using a semi-analytical approach of the positive and negative corona discharge for a wire-to-plate electrode system. Thus, approximate formulas useful for the characterization and control of corona discharge devices are provided, which helps to significantly reduce computational costs. Based on the obtained results, the electro-hydrodynamic (EHD) force generated by the corona discharge has been determined, and it has been used in the Navier-Stokes equations to compute the spatial distribution of the gas velocity. As a result, the influence of the corona plasma region in the flow pattern, particularly in the vicinity of the corona electrode, has been brought to light, which helps to understand the different flow velocities observed in positive and negative coronas. Moreover, the influence of voltage, wire radius, and inter-electrode separation on the electric wind velocity has been investigated.

Keywords: Corona discharge; electric wind; semi-analytical approach; wire-to-plane electrode geometry; fluid model.

1. Introduction

Corona discharge occurs when high voltage is applied between two electrodes, and at least one of them has a sharp curvature. A strong electric field is then created around the sharp electrode, causing a local breakdown and the flow of electric current between the two electrodes. When charged carriers (electrons and ions) traversing the inter-electrode space collide with neutral gas particles, they transmit a part of their momentum to them, which sets the gas in motion. The flow thus generated is generally referred to as electric wind, ion wind or EHD flow. This phenomenon has been known for a long time [1], but it still remains under study due to its complexity. The electric wind can be generated in corona discharges as well as in other types of electric discharges [2], and its mechanism depends on the nature of the discharge itself.

Electric wind has many growing industrial and research applications, such as heat transfer enhancement [3, 4], EHD pumps and micro-pumps [5, 6], EHD flow control [7] and ionic loudspeakers [8]. Moreover, practical devices exploiting electric wind usually have additional advantages over other technologies, including a simple design, small weight and size, no need for moving parts, low cost, and a long lifetime.

In the last decades many theoretical and experimental efforts have been conducted to increase our understanding on the EHD flow produced by corona discharges. For instance, the pioneer model of Robinson [9] related the velocity of the ionic wind to the current intensity of the electric discharge,

which was confirmed in his experiments. Béquin et al. [10] investigated the velocity flow distribution in negative point-to-plane corona in air. They developed a one-dimensional model of neutral particle velocity along the corona discharge axis, and they measured the velocity profiles using Laser Doppler Anemometry (LDA). The discrepancy between the modeling and the measurements were attributed to the omission of the ring vortex formation in the model, and to the perturbation that tracing particles may have on the corona discharge. For the case of positive DC corona discharge, Lacoste et al. [11] were able to estimate the gas velocity using a simplified model, and they compared the model predictions with the measurements obtained using LDA. The measured velocity profile was reasonably fitted by the model, but the radius of the corona plasma region was an adjustable parameter in their model.

More recently, a wide variety of numerical techniques and modeling approaches have been applied to investigate and characterize the generation of ion wind in electric coronas. For example, Zhao and Adamiak [12, 13] used a hybrid numerical algorithm to solve both the Gauss and charge transport equations. Once the EHD force was determined, Navier-Stokes equations were integrated using the finite-volume method in order to evaluate the gas flow. The authors followed an iterative procedure to ensure the consistency between the corona simulation and the fluid flow programs. Ahmedou and Havet [14] have simulated the airflow in a flat duct, in which corona discharge is generated by a single or multiple fine-wire electrodes. The electrical problem (Gauss and charge conservation equations) was coupled to the fluid dynamics problem (mass, momentum and energy conservation equations) and they were solved in the drift region using the finite element method. Since the ionization layer at the vicinity of the wire was not modeled, the authors have to formulate a proper boundary condition for the space charge density on the corona wire. In order to reduce the computational costs, Seimandi et al. [15] have proposed an asymptotic model for steady wire-to-wire corona discharges, in which the inter-electrode space is divided in three regions: two thin ionization regions around the electrodes and one larger ion-drift region. A simplified kinetic model was considered for each region, which allowed the establishment of quasi-analytical solutions for the electric field and the particle fluxes, and to estimate the velocity of the ionic wind from Euler equations. Cagnoni et al. [16] have carried out a numerical study with the aim of modeling the EHD cooling of a condensation radiator. They have applied a staggered solution algorithm to solve the strongly coupled set of partial differential equations that governs the problem. Very recently, Chen et al. [17] have studied numerically and experimentally the ionic wind generation in a point-to-cylinder negative corona discharge operating in the Trichel regime. They observed that flow velocity and the EHD body force have opposite directions in the ionization region, close to the tip, and in the ion drift region, further away from the tip.

In the present work, the generation of EHD wind will be modeled for a parallel wire-to-plate electrode geometry, both for the positive and negative polarities. Corona discharges are time-dependent phenomena, and a complete description of the problem would require solving a fully dynamic numerical model, which demands very long computational times. Therefore, in this study, a stationary or steady-state model will be used to formulate the governing equations of the corona discharge for electrons, positive ions and negative ions. This type of model allows the evaluation of the spatial distribution of time-averaged corona parameters with less numerical effort, and they have been widely used in the scientific literature [15, 18, 19]. The governing equations will be solved semi-analytically, so that simple relations of the time-averaged spatial distributions of ions, electrons and their fluxes are obtained. These approximated solutions are useful in modeling studies and applications of coronas and, in particular, to evaluate the electrical force that originates the EHD motion. Thus, in a second step, the electrical force will be used in the Navier-Stokes equation to compute the 2D spatial distribution of the gas velocity. Special attention will be paid in this study to the ion wind structure in the vicinity of the corona wire for each polarity, as well as to the influence of the geometrical

parameters (wire radius and inter-electrode separation) and electrical parameters (applied voltage) on the ion wind intensity.

The present study is based in previous models of corona discharge, which have been applied to different electrode geometries [18, 20-22]. These models have been validated by comparing their results with other numerical techniques [20, 22] and, indirectly, with the experimental measurements of the ozone produced by the corona discharge [21]. This work also follows the same strategy as that adopted in [23], where the electric wind generated in positive corona discharge was evaluated. However, the emphasis of that work was placed on the effect of the EHD motion on the spatial distribution of the chemical species generated by the corona discharge. In contrast, the goal of the present study is to investigate the differences in the ion wind produced by positive and negative coronas, and how it is affected by geometrical and electrical parameters.

2. Governing equations

The correct assessment of the charged particles densities and of the electric field is essential to have a good approximation of the EHD force acting on the fluid. This force is an input parameter in the Navier-Stokes equations, which ultimately will determine the gas flow profile. Therefore, in this section, the mathematical model of the positive and negative corona discharge will be firstly presented in section 2.1. Then, the expression for the EHD force will be defined in section 2.2. Finally, in section 2.3, the mechanical equations governing the fluid flow will be introduced.

2.1. The corona discharge model

Corona discharge is assumed to take place in air at atmospheric pressure and room temperature using a parallel wire-to-plate electrode configuration. DC high voltage is applied to the wire, while the plate is grounded. The radius of the wire and the distance between the wire and the plate will be designated as r_0 and d, respectively. The electrical discharge is supposed to have translational symmetry in the direction of the wire, so that it can be modeled as a plane 2D problem. Furthermore, it is assumed that the electrical discharge is symmetric with respect to the symmetry axis of the electrode configuration. These assumptions are quite reasonable when modeling positive coronas. However, negative coronas may appear either as a glow, with a very uniform distribution of current, or concentrated into small active spots, which are usually called “tufts” or “beads” [24, 25]. The first mode, termed “ideal corona” by Vann Bush and Snyder, is favored by the used of smoothly polished wire. Therefore, the previous assumptions fit well into this first mode of negative corona.

Corona discharge can be successfully simulated using a fluid approximation, which consists in solving a set of continuity equations for the charged particles coupled with the Gauss equation for the electric field. Usually, only three generic types of charged particles (electrons, positive ions, and negative ions) need to be considered for the physical modelling [26, 27]. In the case of a positive corona, negative ions and electrons spread over a short distance (~10 μm) from the wire [22], but the negative ion density is much weaker than the electron density. Therefore, for the purpose of this work, negative ions can be ignored in the positive corona.

Assuming a stationary discharge, the governing equations can be written as

$$-\nabla \cdot \mathbf{J}_e = (\alpha - \eta)|\mathbf{J}_e|, \tag{1}$$

$$\nabla \cdot \mathbf{J}_p = \alpha |\mathbf{J}_e|, \tag{2}$$

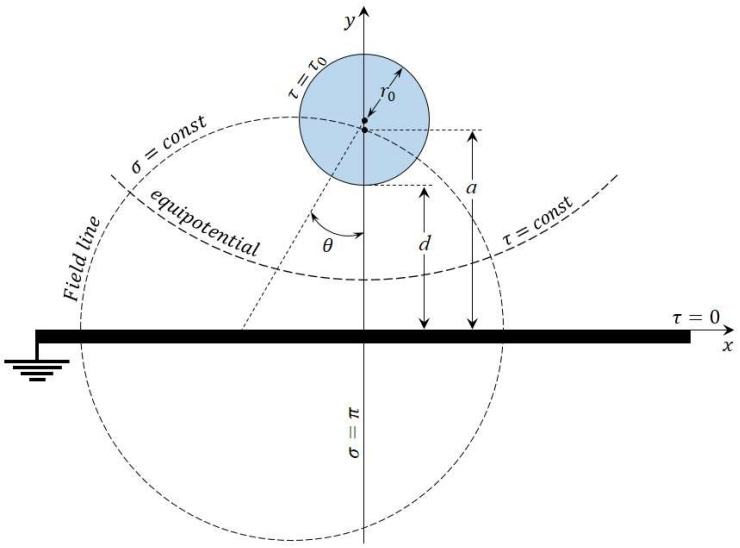

Figure 1. Bipolar coordinates system (σ, τ) used to describe the corona discharge in the wire-to-plate electrode geometry. Coordinate lines are shown as dashed lines. (Not to scale).

$$-\nabla \cdot \mathbf{J}_n = \eta \left| \mathbf{J}_e \right|, \tag{3}$$

$$\nabla \cdot \mathbf{E} = \frac{e_0}{\varepsilon_0}\left(N_p - N_e - N_n \right), \tag{4}$$

where subscripts e, p and n correspond to electrons, positive ions and negative ions; $\mathbf{J}_i$ and N_i denotes the flux and the number density of particles of type i (i = e, p and n), respectively; $\mathbf{E}$ is the electric field, α and η are the ionization and attachment coefficients, respectively; ε_0 is the air permittivity; and e_0 is the elementary charge. The flux of each type is given as $\mathbf{J}_i = \mu_i N_i \mathbf{E}$, where μ_i is the electrical mobility of particle i.

As shown in previous works, bipolar coordinates [28, 29] are particularly adequate to formulate electrostatic problems in wire-plate electrode geometry, since the coordinate curves σ = const. coincides with the Laplacian field lines (figure 1). Therefore, in order to solve semi-analytically (1)-(4), the same strategy as that adopted in [21] for the positive corona will be used here, namely, the electric field lines in the corona discharge will be approximated by the Laplacian field lines. The justification of this approximation lies in fact that field lines computed with more complex models do not differ significantly from Laplacian field lines [30]. The corona discharge model will also be extended to include the case of the negative polarity, and some additional approximations will be introduced later in the vicinity of the wire, which will greatly simplify the solution.

Taking into account the above considerations, the set of equations (1)-(4) can be written using the bipolar coordinates system (σ, τ) as:

$$\mp \frac{1}{S}\frac{d}{dl}\left[SJ_e \right] = \left(\alpha - \eta \right) J_e, \tag{5}$$

$$\pm \frac{1}{S}\frac{d}{dl}\left[SJ_p \right] = \alpha J_e, \tag{6}$$

$$\mp \frac{1}{S}\frac{d}{dl}\left[SJ_n \right] = \eta J_e, \tag{7}$$

$$\pm \frac{1}{S}\frac{d}{dl}\left[SE \right] = \frac{e_0}{\varepsilon_0}\left(N_p - N_e - N_n \right), \tag{8}$$

where the upper (lower) sign is for positive (negative) corona, E is the magnitude of the electric field; $J_i = \mu_i N_i E$ is the magnitude of the flux of i-th particles; $dl = -Sd\tau$ is the infinitesimal displacement along the electric field line (σ = const.) in the direction of the plate, and S is the scale factor of coordinates σ and τ. The equations defining the scale factor and the correspondence between Cartesian and bipolar coordinates are

$$S = \frac{a}{\cosh\tau - \cos\sigma}, \quad x = \frac{a\sin\sigma}{\cosh\tau - \cos\sigma}, \quad y = \frac{a\sinh\tau}{\cosh\tau - \cos\sigma}, \tag{9}$$

where distance a is related to the wire radius, r_0, and the electrode separation, d, as $a = \sqrt{(d + r_0)^2 - r_0^2}$. Note that $a \approx d$ for a thin wire ($r_0 \ll d$).

The ionization and attachment coefficients to be used in (5)-(7) have been fitted from the data provided by Bolsig [31, 32] for air as follows,

$$\alpha = A_1 \exp\left(-\frac{B_1}{E}\right), \quad \left(1.1\times10^4 \le E \le 2.0\times10^5 \text{V/cm}\right) \tag{10}$$

$$\eta = \alpha_1 + \alpha_2 E + \alpha_3 E^2 + \alpha_4 E^3, \quad \left(1.1\times10^4 \le E \le 2.0\times10^5 \text{V/cm}\right) \tag{11}$$

where A_1 = 6.4×10^3 cm^{-1}, B_1 = 1.9×10^5 Vcm^{-1}, α_1 = 13.60 cm^{-1}, α_2 = −8.20×10^{-5} V^{-1}, α_3 = −7.78×10^{-12} V^{-2} cm and α_4 = 1.042 ×10^{-15} V^{-3} cm^2.

From the continuity equations (5)-(7), it can be shown that the product JS, where $J = J_e + J_p + J_n$, is a constant along the field lines,

$$JS = \text{const.} \tag{12}$$

Therefore, the current density measured at the wire, $j_0 = e_0 J_0$, and at the plate, $j_T = e_0 J_T$, can be linked to each other as

$$j_0 = j_T \frac{S_T}{S_0} = j_T \frac{\cosh\tau_0 - \cos\sigma}{1 - \cos\sigma}, \tag{13}$$

where subscripts 0 and T denote that the corresponding quantities are evaluated on the wire and the plate, respectively. The corona current distribution over the ground plate, j_T, is formulated from Warburg's law [33, 34] as

$$j_T = j(0)\cos^m\theta = j(0)\left[\frac{(d + r_0)(1 - \cos\sigma)}{\sqrt{(a\sin\sigma)^2 + (d + r_0)^2(1 - \cos\sigma)^2}}\right]^m, \tag{14}$$

where m = 4.5 (m = 4.65) for positive (negative) corona, and $j(0)$ is the current density at the center of the plate (on the axis of symmetry). The value $j(0)$ can be determined from the total current I as follows,

$$I = 2\int_0^\infty j_T w dx = 2(d + r_0) w j(0) \int_0^{\pi/2} \cos^{m-2}\theta d\theta \approx d\, w j(0) K, \tag{15}$$

where w is the length of the wire and K = 1.44 (K = 1.40) for positive (negative) corona.

Following the approach of Chen and Davison [18], the space between the electrodes can be split into two different zones: the *corona plasma region* and the *drift region.* Ionization, electron attachment, and electron-induced chemical reactions take place within the corona plasma region, in the vicinity of the wire. The drift region extends from the outer boundary of the plasma region up to the ground

electrode. No further plasma activity occurs in drift region, since the number density of electrons is small. Therefore, in this zone, ions injected from the corona plasma region drift towards the collecting plate under the effect of the electric field. The boundary between the plasma region and the drift region must be situated at a distance from the wire where the density of electrons is sufficiently weak.

Since the wire diameter is very small compared with the electrode separation, bipolar coordinates can be approximated by polar coordinates inside the corona plasma region. Therefore, the scale factor S becomes $S \approx r(S_0/r_0)$, with r the radial distance to the centre of the wire, and the infinitesimal displacement along the electric field line satisfies $dl \approx dr$. This approximation will greatly simplify the solution of (5)-(8) in the plasma region.

2.1.1 Electric field

As shown in previous studies [22], most of the space charge accumulates in the drift region. Therefore, the time-averaged electric field distribution in the plasma region can be obtained by integrating (8) without space charge, which gives

$$E = \frac{E_0 S_0}{S} \approx \frac{E_0 r_0}{r}, \tag{16}$$

where subscript 0 refers to the wire.

In the drift region, the space charge is mainly constituted by ions with the same polarity as that of the corona wire, that is, $N_i = J_i/(\mu_i E) = J_T S_T/(\mu_i E S)$, where $i = p$ in the positive corona, and $i = n$ and in the negative corona. Therefore, integration of (8) gives [21],

$$E(\sigma,\tau) = \frac{1}{S(\sigma,\tau)}\left[(S_0 E_0)^2 - c_i \frac{a^3/\sin^2\sigma}{1-\cos\sigma}\left(\frac{2}{\tan\sigma}\tan^{-1}\left[\left(\frac{1+\cos\sigma}{\sin\sigma} \right)\tanh\left(\frac{\tau}{2} \right) \right] + \frac{\sinh\tau}{\cosh\tau - \cos\sigma} \right)_{\tau_0}^{\tau} \right]^{\frac{1}{2}}, \tag{17}$$

where $c_i = 2j_T/(\varepsilon_0 \mu_i)$ and E_0 is the electric field on the wire surface, which can be estimated using Peek's law [35]. This expression of the electric field can actually be used in whole inter-electrode space, since the contribution of the second addend inside the square root becomes negligible in the corona plasma region, where $\tau \approx \tau_0$, and (17) becomes (16).

2.1.2 Electron flux

Since electrons are confined to the plasma region, bipolar coordinates can be approximated by polar coordinates, and the ionization and attachment coefficients can be written as

$$\alpha \approx A_1 \exp(-B_2 r), \tag{18}$$

$$\eta \approx a_1 + \frac{a_2}{r} + \frac{a_3}{r^2} + \frac{a_4}{r^3}, \tag{19}$$

where $B_2 = B_1/(E_0 r_0)$, $a_1 = \alpha_1, a_2 = \alpha_2(E_0 r_0)$, $a_3 = \alpha_3(E_0 r_0)^2$ and $a_4 = \alpha_4(E_0 r_0)^3$. Then, the flux of electrons can be obtained by direct integration of (5)

$$J_e = \frac{S_0 J_{e0}}{S}\exp\left[\mp\int_0^l (\alpha - \eta)\, dl' \right] \approx \frac{S_0 J_{e0}}{S}\exp\left[\mp\int_{r_0}^r (\alpha - \eta)\, dr' \right] = J_{e0} f(r), \tag{20}$$

where

$$f(r) = \left(\frac{r_0}{r} \right)^{1\mp a_2} \exp\left[\pm\frac{A_1}{B_2}\left(\exp(-B_2 r) - \exp(-B_2 r_0) \right) \pm a_1 (r - r_0) \mp a_3 \left(\frac{1}{r} - \frac{1}{r_0} \right) \mp \frac{a_4}{2}\left(\frac{1}{r^2} - \frac{1}{r_0^2} \right) \right] \tag{21}$$

and J_{e0} is the electron flux on the wire surface. As usual, the upper (lower) sign corresponds to positive (negative) corona.

2.1.3 Positive ion flux

Within the plasma region, the flux of positive ions can be obtained from (6) as follows

$$J_p = \frac{S_0}{S} J_{p0} \pm \frac{1}{S} \int_0^l S\alpha J_e dl' \approx \frac{r_0}{r} J_{p0} \pm \int_{r_0}^r A_1 r' \exp\left(-B_2 r'\right) J_{e0} f(r') dr' , \tag{22}$$

where J_{p0} is the flux of positive ions on the wire. In the positive corona, it must be $J_{p0} = 0$, owing to the polarity of the wire. In the negative corona, the current on the wire is contributed by positive ions and electrons, but $J_{p0} \gg J_{e0}$. Therefore $J_0 \approx J_{p0}$, and flux of positive ions on the wire can be linked to the current on the plate using (13)

$$J_{p0} \approx \frac{1}{e_0} j_T \frac{S_T}{S_0} . \tag{23}$$

Equation (22) is particularly useful in the case of a negative corona, since positive ions are confined to the plasma region. However, in a positive corona, positive ions accumulate in the drift region. In such a case, a more straightforward evaluation of the positive ion flux can be obtained using (12)

$$J_p = \frac{S_T J_T}{S} - J_e , \tag{24}$$

which further simplifies in the drift region to $J_p \approx S_T J_T / S$, since $J_p \gg J_e$.

2.1.4 Negative ion flux

As stated previously, in the positive corona, the number density of negative ions is much weaker than that of electrons, and they are confined to a short distance from the wire. Therefore, they will not contribute significantly to the electric force and will be omitted in the present study. In contrast, in the negative corona, negative ions are present both in the corona plasma region and in the drift region. In the corona plasma region, the flux of negative ions can be deduced from (7) as

$$J_n = \frac{S_0}{S} J_{n0} + \frac{1}{S} \int_0^l S\eta J_e dl' \approx \frac{1}{r} \int_{r_0}^r r' \left(a_1 + \frac{a_2}{r'} + \frac{a_3}{r'^2} + \frac{a_4}{r'^3} \right) J_{e0} f(r') dr' , \tag{25}$$

where it has been taken into account that $J_{n0} = 0$, due to the polarity of the wire.

However, once the electron flux and the positive ion flux have been previously determined, a more convenient relation can be obtained using (12),

$$J_n = \frac{J_T S_T}{S} - J_p - J_e , \tag{26}$$

which is valid in the whole discharge gap. In the drift region, where $J_n \gg J_e$ and $J_n \gg J_p$, the above equation can be approximated as $J_n \approx S_T J_T / S$.

2.1.5 Electron flux on the corona wire

The value of the electron flux on the corona wire, J_{e0}, is required in (20), (22) and (25) in order to evaluate J_e, J_p and J_n, respectively.

In the positive corona, the flux of positive ions on the wire must be null ($J_{p0} = 0$) and, as explained before, the flux of negative ions can be ignored compared to the flux of electrons. Therefore, the electron flux on the wire surface can be linked to the total current density on the plate using (13)

$$J_{e0} = \frac{1}{e_0} j_T \frac{S_T}{S_0} . \tag{27}$$

However, in the negative corona, positive ions constitute the major contributors to the current density on the wire. Thus, a different strategy must be followed in order to determine the electron flux on the corona electrode. The electron current reaches its maximum value in the corona plasma region when the ionization coefficient equals the attachment coefficient, $\alpha = \eta$, which corresponds to an electric field strength $E_L \approx 30$ kV/cm and to a radial distance $r_L \approx E_0 r_0 / E_L$. At this location, the positive and negative ion currents are very similar, so that $J_n(r_L) \approx J_p(r_L)$, and the total current density can be linked to that on the plate using (12)

$$e_0 J_T S_T = e_0 \left(J_e(r_L) + J_p(r_L) + J_n(r_L) \right) S_L \approx e_0 \left(J_e(r_L) + 2J_p(r_L) \right) S_L . \tag{28}$$

This equation can be used as condition to determine the electron density on the wire surface. Substitution of (20) and (22) in (28) leads to

$$J_{e0} = \frac{r_0 J_T S_T / S_0}{2\left[\int_{r_0}^{r_L} A_1 r \exp\left(-B_2 r'\right) f(r') dr' \right] - r_L f(r_L)} . \tag{29}$$

2.2. The EHD force expression

Charged particles generated in the corona discharge are accelerated by the electric field and gain kinetic energy. Moreover, they transfer their momentum to the surrounding neutral gas molecules through collisions, which results in a bulk gas flow. According to Boeuf's approach [36], and assuming that the air motion has a negligible influence on the corona discharge, the EHD force density acting on the fluid can be expressed as

$$\mathbf{F} = e_0 \left(N_p - N_n - N_e \right) \mathbf{E} . \tag{30}$$

Since $\mathbf{J}_i = \mu_i N_i \mathbf{E}$ ($i = e$, p and n), the electric force can also be written as a function of the flux of charged species,

$$\mathbf{F} = e_0 \left(\frac{\mathbf{J}_p}{\mu_p} - \frac{\mathbf{J}_n}{\mu_n} - \frac{\mathbf{J}_e}{\mu_e} \right). \tag{31}$$

2.3. Gas flow model

The fluid flow can be described by Navier-Stokes equation and the continuity equation, which represent the conservation of momentum and mass, respectively. Assuming that the air motion can be approximated as an incompressible Newtonian flow, these equations can be written as

$$\frac{\partial \mathbf{V}}{\partial t} + \left(\mathbf{V} \cdot \nabla \right) \mathbf{V} = \eta \Delta \mathbf{V} - \nabla p + \frac{\mathbf{F}}{\rho}, \tag{32}$$

$$\nabla \cdot \mathbf{V} = 0, \tag{33}$$

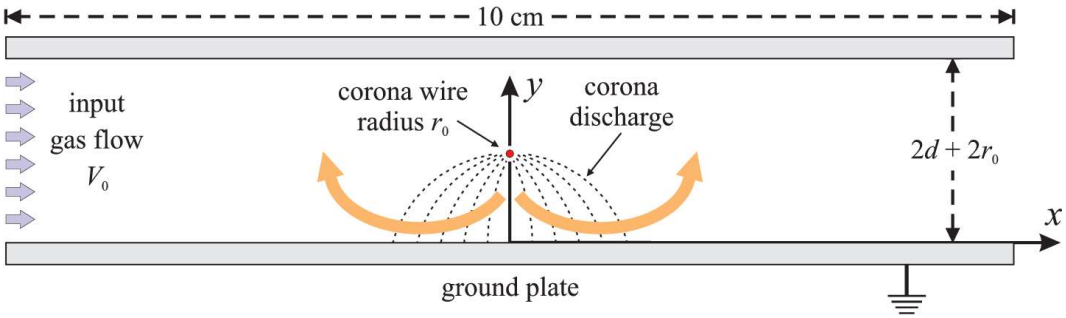

Figure 2. Schematic picture of the wire–plate corona reactor.

where **V** is the gas velocity, η is the kinematic air viscosity, p is the gas pressure, and ρ is the air density.

In this work, the flow is assumed to be confined between two parallel plates, with the bottom plate (the ground electrode) located at $y = 0$ and the top plate at $y = 2d + 2r_0$ (see figure 2). The channel width is taken as 10 cm, the entrance being situated at $x = -5$ cm and the exit at $x = 5$ cm. The length of the channel, along the z-direction, is assumed to be infinite. The corona wire runs parallel to the z-axis, with its center at the coordinates $x = 0$ and $y = d + r_0$.

Boundary conditions for the airflow are straightforward. Firstly, no-slip conditions are imposed at the plates and at the wire surface. At the entrance of the channel ($x = -5$ cm), the gas flow is assumed to be parallel to the x-direction, with a constant velocity V_0. At the exit ($x = 5$ cm), the gas pressure is imposed to be equal to the atmospheric gas pressure.

The electrohydrodynamic motion induced by the corona discharge will be, in general, turbulent [12, 14]. Therefore, the usual approach of time-averaging the conservation equations of momentum and mass, which leads to the so called Reynolds-Averaged Navier–Stokes (RANS) equations, has been followed here. The resulting system of partial differential equations has then been closed using the standard k-ε two-equation model of turbulence [37]. Thus, the turbulent viscosity, η_t, the turbulent kinetic energy, k, and its rate of dissipation, ε, are linked through the relation $\eta_t = C_\mu \rho k^2/\varepsilon$, with $C_\mu = 0.09$, Prandtl numbers σ_k and σ_ε have been given the values $\sigma_k = 1.00$ and $\sigma_\varepsilon = 1.30$, and constants $C_{1\varepsilon}$ and $C_{2\varepsilon}$ of the model are set as $C_{1\varepsilon} = 1.44$ and $C_{2\varepsilon} = 1.92$ [37].

The resulting system of equations has been solved for the stationary regime with the help of the computational fluid dynamics software FLUENT [38], which uses the finite volume method. For that purpose, the pressure-based solver SIMPLE (Semi-Implicit Method for Pressure-Linked Equations) has been applied.

3. Results

3.1 EHD force and ion wind velocity

The numerical results presented in this section have been obtained for a corona wire of radius $r_0 = 100$ μm and an inter-electrode separation $d = 0.5$ cm. The positive and negative high voltage applied to the corona wire have been chosen as $\phi = \pm 8$ kV, to which corresponds a current intensity per unit of wire length of 30.11 μA/cm and −37.6 μA/cm, respectively [39, 30]. As we are mainly interested in studying the effect of the EHD contribution to the air motion, the gas velocity at the entrance of the channel was assigned a small value, $V_0 = 2.5$ cm/s. In any case, the fluid flow within the channel will be turbulent, because the ion wind velocity generated by the discharge of the corona is substantially higher than V_0.

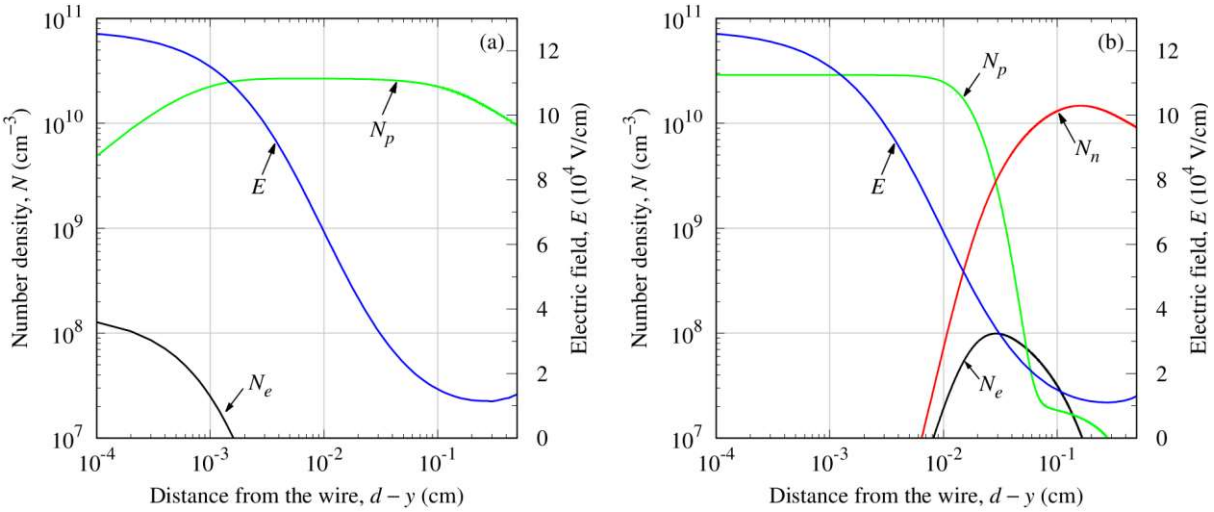

Figure 3. Number densities of charged species (N_p: positive ions, N_n: negative ions and N_e: electrons) and electric field, E, along the axis of symmetry as a function of the distance from the wire, for r_0 = 100 μm and d = 0.5 cm. (a) Positive corona, ϕ = +8 kV. (b) Negative corona, ϕ = −8 kV.

Before illustrating the behavior of the EHD force, it is convenient to first present the profiles of the electric field and of the densities of the charged particles, since the EHD force is related to these physical quantities through (30). The electric field can be calculated at any point of the inter-electrode space using (17). For simplicity, only the electric field distribution along the axis of symmetry is presented in figure 3. Clearly, the electric field intensity is very high near the wire (~1.26×10^5 V/cm), and decreases very rapidly in the direction of the plane, where it takes a value around 1.3×10^4 V/cm. Therefore, the electric field will tend to bring about a greater acceleration to the fluid particles located near the wire, within the corona plasma region, than to those situated further away, in the drift region. A close inspection of figure 3 reveals that the minimum value of the electric field is reached a few millimeters above the plane. This is a consequence of the accumulation of space charge, which slightly reinforces the electric field on the ground electrode. According to the model, the electric field intensity is not greatly affected by the polarity of the corona discharge. On the wire, the electric field is fixed by Peek's law. In the drift region, the mobility of ions could affect the electric field intensity through the parameter c_i. However, since the mobilities of positive and negative ions in air are not very different ($\mu_p = 2\times10^{-4}$ m^{2}V^{-1}s^{-1} and $\mu_n = 2.5\times10^{-4}$ m^{2}V^{-1}s^{-1}), this influence in very weak: at the plate, the electric field in the positive corona is about 4% higher than that in the negative corona.

Figure 3 also shows the number densities of ions and electrons along the axis of symmetry. The spatial distribution of these species is very different in the positive and negative coronas. In the positive corona (figure 3a), electrons drift towards the wire, where the electric field intensity is maximum. In their path, inelastic collisions with neutral molecules cause ionization and the production of secondary electrons. Therefore, the number density of electrons grows very fast and gets its highest value on the wire. Due to the direction of migration of electrons, the region where electrons are present in a significant number is restricted to a few tens of microns form the wire. Moreover, since electron attachment is not favored by intense electric fields, the density of negative ions is much smaller than that of electrons, and they can be ignored in a first approach. Positive ions are also generated during the ionization events, and drift towards the ground plate. However, the mobility of positive ions is about two orders of magnitude smaller than the mobility of electrons. Thus, whilst electrons are rapidly swept out through the wire, positive ions escape much more slowly from the ionization region.

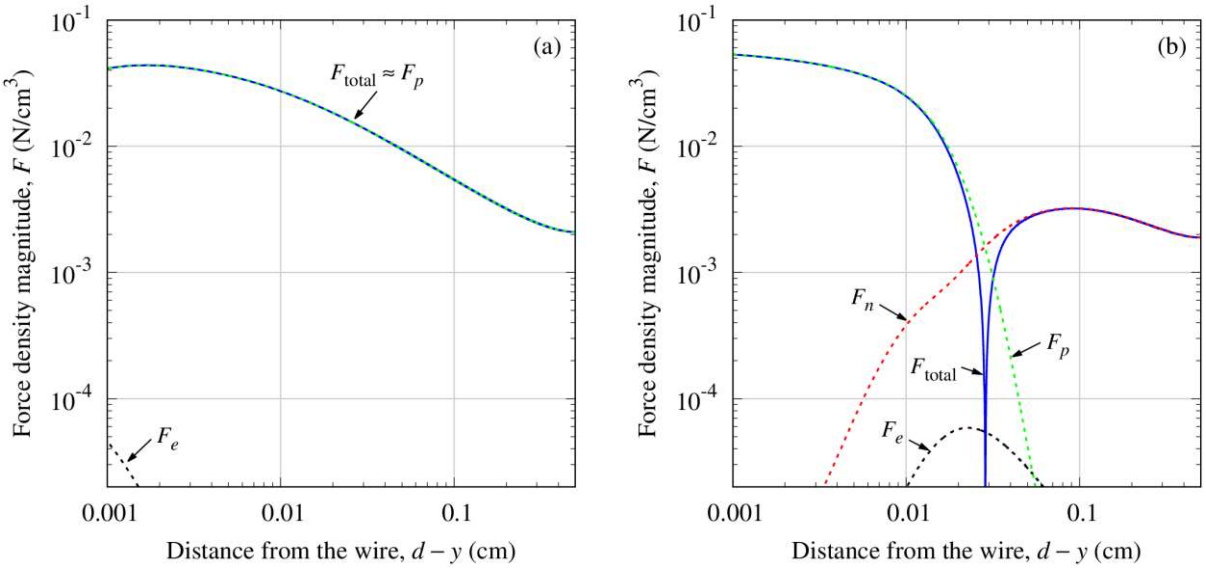

Figure 4. Magnitude of the EHD force density along the axis of symmetry as a function of the distance from the wire, for r_0 = 100 μm and d = 0.5 cm. The total force density, F_{total} , is shown as a solid blue line. The contributions to the force density of electrons (F_e), positive ions (F_p) and negative ions (F_n) are represented by means of dashed lines. (a) Positive corona, ϕ = +8 kV. (b) Negative corona, ϕ = −8 kV.

As a consequence, the number density of positive ions is substantially higher than that of electrons in most of the ionization region.

In contrast, in the negative corona (figure 3b), the number density of electrons increases towards the anode until electron attachment equals ionization, which occurs at a distance of about 0.03 cm from the wire. Beyond that point, the electron number density starts declining. Positive ions formed by ionization drift towards the cathode (the wire), where its number density becomes maximum. Conversely, negative ions formed by electron attachment drift towards the ground plate, although the largest density occurs a few millimeters above the plate, due to the electric field distortion produced by the space charge. In the drift region, the number density of negative ions in the negative corona is similar to that of positive ions in the positive corona.

Figure 4 shows the contributions of ions and electrons to the EHD force along the axis of symmetry, as well as the magnitude of the total EHD force. In the case of a positive corona, the boundary condition for positive ions imposes that its density must vanish at the wire. Therefore, on the wire surface and its close vicinity, the contribution of electrons to the total electrical force must greater than that of positive ions. However, the extent of that region is negligibly small: at 10 μm away from the wire surface, the electric force due the positive ions is already three orders of magnitude higher than that due to electrons (figure 4a). Thus, in the positive polarity, the electrical force acting on the fluid can be entirely assigned to the positive ions, and it is always directed towards the plate.

In the negative corona (figure 4b), the contribution of electrons to the total EHD force is also negligible, since the number density of electrons is, at least, two orders of magnitude smaller than the densities of positive and negative ions. Therefore, in the ionization region, the EHD force is primarily due to the positive ions, and the highest force density is reached on the cathode (~ 5.7×10^{-2} N/cm^3). On the contrary, in the drift region, negative ions are the major contributors to the EHD force. However, the electric field intensity in the drift region is about one order of magnitude lower than in the ionization region and, thus, the EHD force is correspondingly weaker, although it affects a larger area. It must be noted that the EHD force has opposite directions in each region, and it vanishes where ionization and attachment becomes similar (~ 3×10^{-2} cm): in the ionization region, the EHD force is

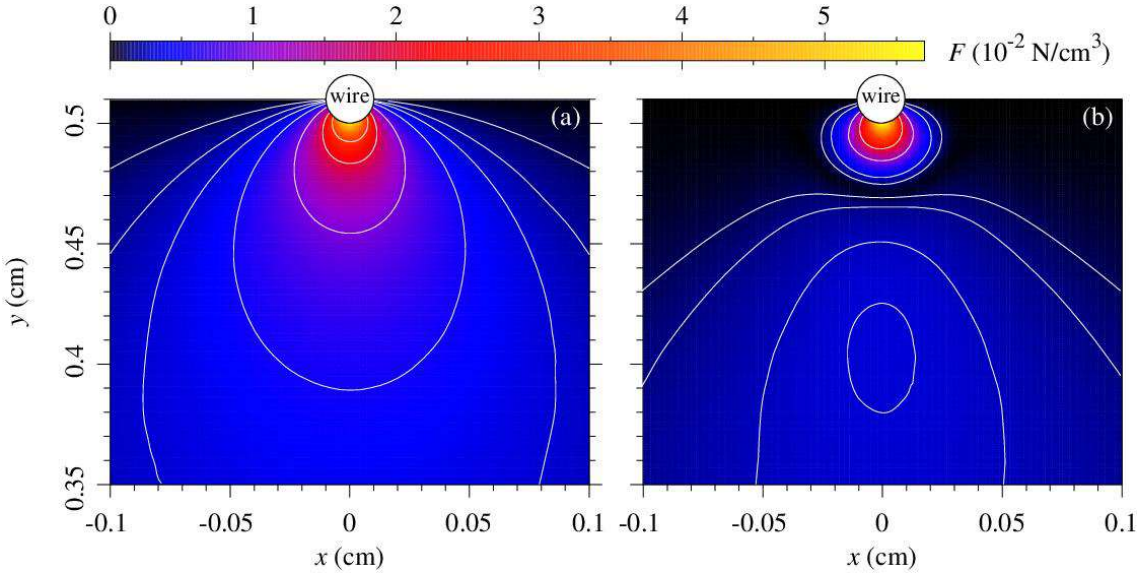

Figure 5. 2D-spatial distribution of the EHD force magnitude in the vicinity of the wire for $r_0 = 100$ μm and $d = 5$ mm. (a) Positive corona, $\phi = +8$ kV. Contour lines are drawn at (0.1, 0.2, 0.3, 0.5, 1, 2, 3) $\times 10^{-2}$ N/cm^3. (b) Negative corona, $\phi = -8$ kV. Contour lines are drawn at (0.1, 0.25, 1, 2) $\times 10^{-2}$ N/cm^3 in the ionization region, and at (0.1, 0.15, 0.25, 3) $\times 10^{-3}$ N/cm^3 in the drift region.

directed towards the wire, while in the negative drift region the EHD force pushes the fluid towards the plate.

Figures 5-7 show the 2D spatial distributions of the EHD force density around the wire, within a rectangular region with height about 30% of the electrode gap. The magnitude of the electric force is presented in figure 5, while the *x*-component and the *y*-component of the force density are shown separately in figures 6 and 7. These figures complete and extend to two-dimensions the information already given in figure 4 along the axis of symmetry. As expected, the EHD force in the positive corona is always directed from the wire to the plate. In contrast, in the negative corona, the electric force exhibits a sign reversal around the boundary where electron attachment takes over from ionization: in the negative charged drift region, the fluid is impelled towards the plate, while in the ionization region it is pushed towards the wire. The closed contour lines in the drift region shown in figures 5b and 7b evince the region where the electric force reaches a maximum in the negative corona. In that same position, the electric force in positive corona is about 1.8 times higher. This difference decreases as the plate is approach, although in the positive corona the EHD force intensity is always superior.

Based on the results of the modeling, asymptotic expressions of the EHD force can be obtained for those regions where the force is predominantly due a single type of ion, either positive or negative. Using (12) and (14), and taking into account (9) and(15), the EHD force can be approximated as

$$F_i = \frac{1}{\mu_i} e_0 J_i \approx \frac{1}{\mu_i} j_T \frac{S_T}{S} = \frac{I/w}{\mu_i K d} \left[\frac{(d + r_0)(1 - \cos\sigma)}{\sqrt{a^2 \sin^2\sigma + (d + r_0)^2 (1 - \cos\sigma)^2}} \right]^m \frac{\cosh\tau - \cos\sigma}{1 - \cos\sigma}, \qquad (34)$$

where $i = p, n$.

In positive corona, this expression can be used to evaluate the electric force in the entire discharge gap since, according to the results already presented in figure 3a, $N_p \gg N_e$, and therefore $F \approx F_p$.

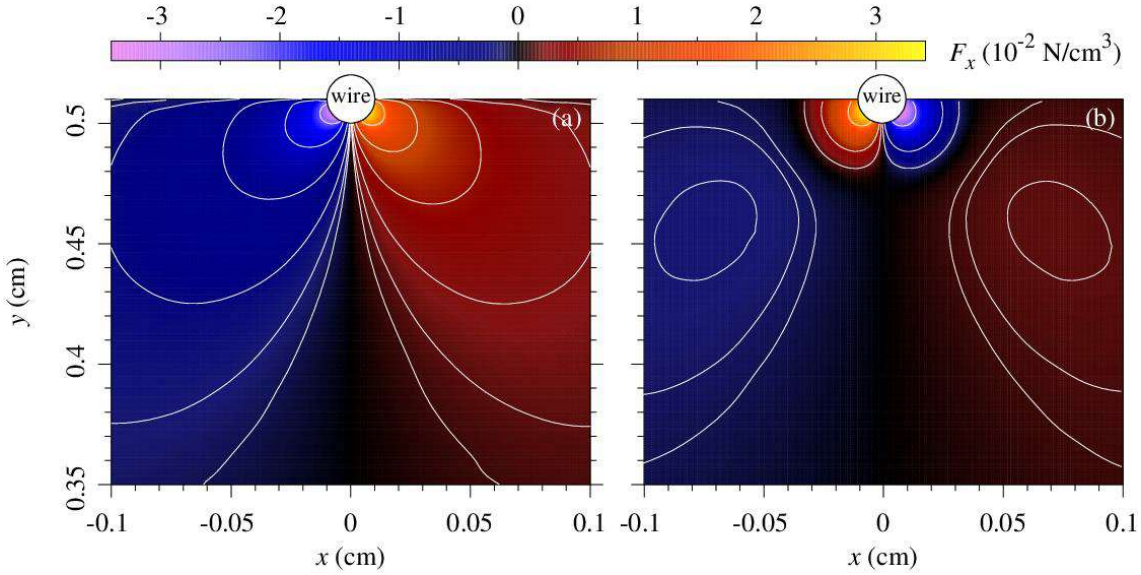

Figure 6. 2D-spatial distribution of x-component of the EHD force in the vicinity of the wire for $r_0 = 100$ μm and $d = 5$ mm. (a) Positive corona, $\phi = +8$ kV. Contour lines are drawn at (±2, ±1, ±0.5, ±0.15, ±0.1) $\times 10^{-2}$ N/cm^3. (b) Negative corona, $\phi = -8$ kV. Contour lines are drawn at (±2, ±0.5, ±0.12) $\times 10^{-2}$ N/cm^3 in the ionization region, and at (±1.5, ±1.2, ±1) $\times 10^{-3}$ N/cm^3 in the drift region.

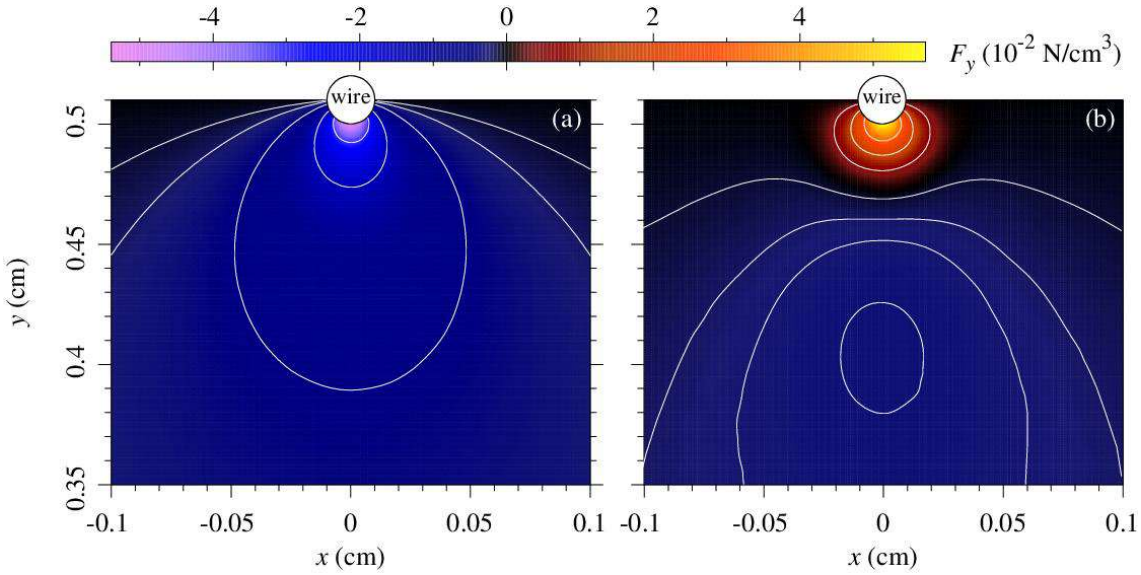

Figure 7. 2D-spatial distribution of y-component of the EHD force in the vicinity of the wire for $r_0 = 100$ μm and $d = 5$ mm. (a) Positive corona, $\phi = +8$ kV. Contour lines are drawn at (3, 1.5, 0.5, 0.2, 0.1) $\times 10^{-2}$ N/cm^3. (b) Negative corona, $\phi = -8$ kV. Contour lines are drawn at (3, 1.5, 0.5) $\times 10^{-2}$ N/cm^3 in the ionization region, and at (−1, −2, −2.5, −3) $\times 10^{-3}$ N/cm^3 in the drift region.

Regarding negative corona, positive ions were preponderant in the proximity of the wire (figure 3b). In section 2.1.5, $E_L \approx 30$ kV/cm was defined as the electric field corresponding to $\alpha = \eta$. Therefore, $E_1 \sim 2E_L \approx 60$ kV/cm can be set as lower bound above which ionization and positive ions prevail. This criterion is met for radial distances shorter than $r_1 \approx E_0 r_0 / E_1 \approx 200$ μm. Thus, for $r < r_1$ it must be $N_p \gg N_n$ and $N_p \gg N_e$, and (34) can be used to obtain the EHD force, since $F \approx F_p$.

On the contrary, in the drift region of the negative corona, negative ions dominate (figure 3b). The electric field strength $E_2 \sim E_L/2 \approx 15$ kV/cm can be set now as an upper bound below which electron

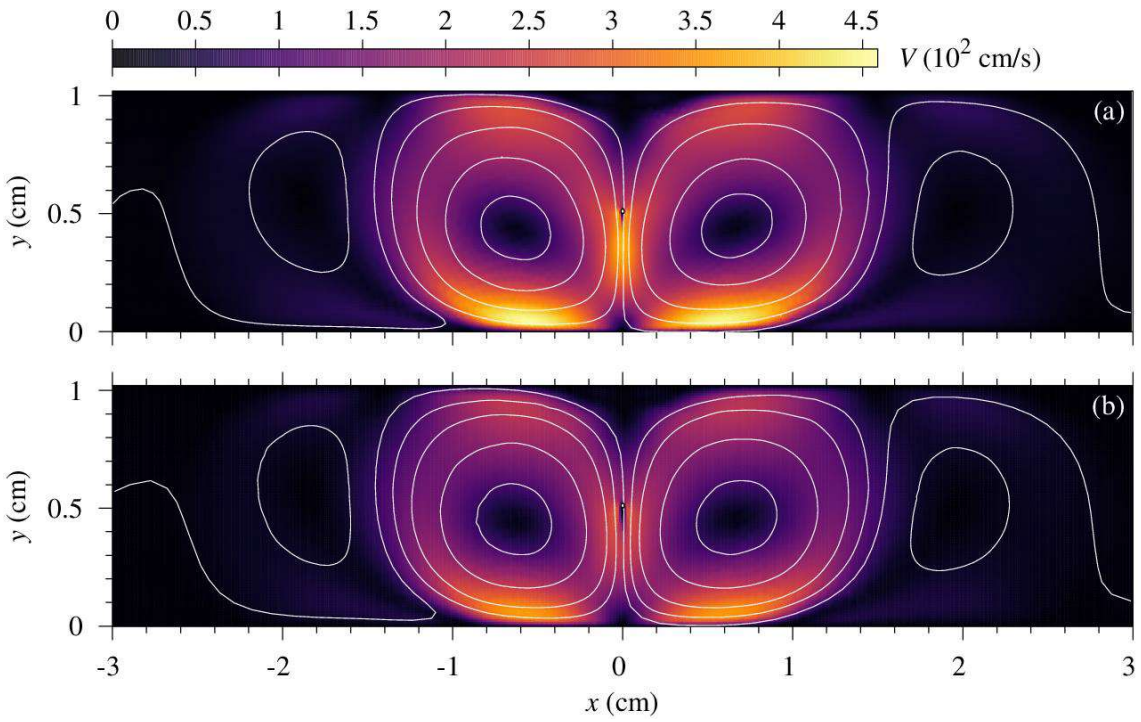

Figure 8. 2D-spatial distribution of the gas velocity magnitude between the two parallel plates for r_0 = 100 µm and d = 0.5 cm. Streamlines are drawn as white solid lines. (a) Positive corona, ϕ = +8 kV. (b) Negative corona, ϕ = −8 kV. The corona wire is situated at the center of each plot.

attachment to form negative ions prevails over ionization. This condition is satisfied at radial distances longer than $r_2 \approx E_0 r_0 / E_1 \approx 800$ µm. Thus, for $r > r_2$ it must be $N_n \gg N_p$ and $N_n \gg N_e$, and (34) can again be used to obtain the EHD force, since $F \approx F_n$.

In between the two zones ($r_1 < r < r_2$), both positive and negative ions contribute to the EHD force in the negative corona, and (34) cannot be used. However, since F_p and F_n have opposite directions, the net EHD force will have a small value (figure 4b).

Figure 8 shows the spatial distribution of the gas velocity between the plates originated by the positive (figure 8a) and the negative (figure 8b) corona discharge, alongside with the streamlines, for an applied voltage of ±8 kV. Since the corona plasma region is limited to a thin layer around the wire, the flow distribution depicted in figure 8 is mainly driven by the EHD force acting in the drift region. This force accelerates the fluid from the corona wire towards the plate, where the flow is deflected along the wall in opposite directions. Thus, the stationary flow pattern is organized as two nearly symmetrical rolls, with their centers located about 1 mm below the wire and 5 mm on either side of the wire. The structure of the flow is similar in both coronas, but the flow velocity is higher in the case of the positive corona. The maximum values of the air velocity, about 4.6 m/s in the positive corona and 3.6 m/s in the negative corona, are found in the deflected flow that circulates parallel to the lower plate. In any case, the gas velocities reported here are two orders of magnitude lower than the ions velocity. This fact justifies the approximation of neglecting the interaction between the corona discharge and the gas flow [12].

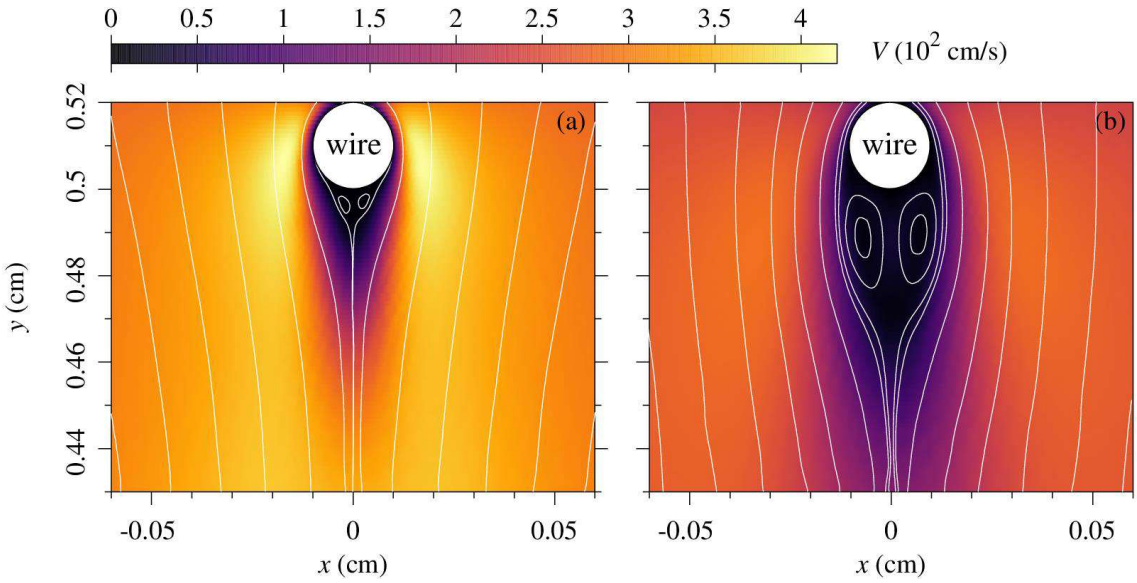

Figure 9. 2D-spatial distribution of the gas velocity magnitude in the vicinity of the corona wire for $r_0 = 100$ µm and $d = 0.5$ cm. Streamlines are drawn as white solid lines. (a) Positive corona, $\phi = +8$ kV. (b) Negative corona, $\phi = -8$ kV.

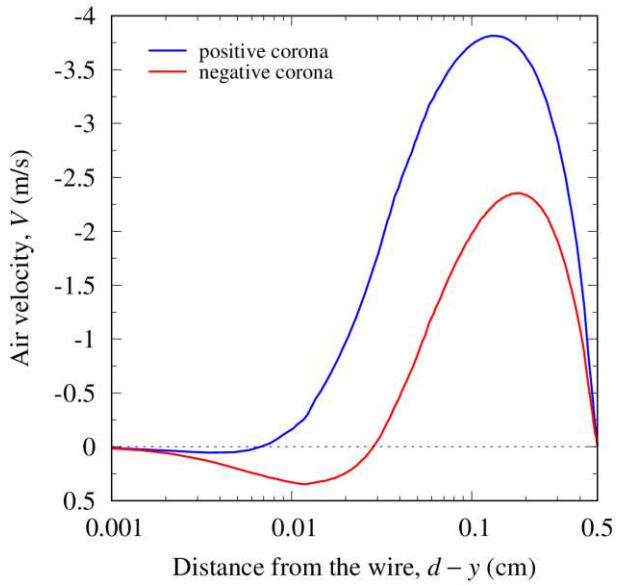

Figure 10. Gas velocity magnitude along the axis of symmetry ($x = 0$) in positive and negative corona for $r_0 = 100$ µm, $d = 5$ mm and $\phi = \pm 8$ kV.

A detailed view of the gas flow in the proximity of the wire is shown in figure 9. As it is well known, at moderate Reynolds numbers, the flow structure in the downstream region of a cylinder is characterized by the presence of two recirculating and stable vortices behind the cylinder, which have a hydrodynamic origin [40]. Therefore, a similar pattern can be expected to develop in the corona discharge, beneath the wire, due to the mainstream flow coming from above the corona wire. However, in the positive corona, the space charge is mostly positive, even in the vicinity of the wire, so that the fluid is always impelled towards the plate. Thus, the development of these vortices is strongly inhibited by the electric force, and they have a reduced size and velocity (see figure 9a). In contrast, in the negative corona, the ionization generates a positive charge layer in front of the wire, of about 300 µm, which pushes the fluid towards the wire. As a result, the formation of the two vortices

is favored, and they have a much larger size and velocity than in the positive corona. The maximum velocity, $V \approx 34$ cm/s, is reached on the symmetry axis. Although this velocity is smaller than the ones observed in the drift region, the corresponding velocity gradients are larger.

Figure 10 highlights the differences in the EHD induced velocity along the symmetry axis between the positive and a negative corona discharge. The air velocity is zero at the corona wire and at the ground plate, due to the non-slip condition. However, the gas velocity increases faster and reaches a higher speed ($V_{max} \approx 3.8$ m/s) in the positive corona than in the negative corona ($V_{max} \approx 2.3$ m/s). Also, in the positive corona, the point where the maximum speed is attaint is closer to the wire.

The prediction of the model of a higher gas velocity in the positive corona is in agreement with the experimental observations of Kozlov and Solovyov [41] and other investigators. As explained by these authors, the ionic wind velocity depends on the ion mobility (the larger the ion mobility the lower the ionic wind velocity) and the mobility of positive ions is lower than that of negative ones ($\mu_p = 2\times10^{-4}$ $m^2V^{-1}s^{-1}$ and $\mu_n = 2.5\times10^{-4}$ $m^2V^{-1}s^{-1}$ in this work). However, according to the results of the present study, the structure of the corona plasma region is another important factor that needs to be taken into account: in the negative corona, the EHD force changes its direction from the ionization to the drift region and, therefore, the fluid is accelerated towards the plate less efficiently than in the case of a positive corona.

Comparison with experiments

In this subsection, modeling results are compared with the experimental measurements reported by Elagin et al. [4] for a parallel wire-plate electrode configuration. They used the particle image velocimetry (PIV) method to visualize the flow, and the purpose of their study was to investigate the cooling enhancement produced by the ionic wind. Therefore, the plate was set horizontally below the wire, and it was heated to a steady temperature of about 65 K above the ambient temperature. However, since the gas velocity due to natural convection was very small compared to that produced by the ion wind, the velocity pattern and velocity values measured by the PIV technique are essentially due to EHD gas motion. Furthermore, in their experiments, negative corona was characterized by the presence of localized “tufts” along the wire, which, as previously mentioned, is not compatible with the assumptions of the model. As a result, ionic wind jets emitted from these localized spots resulted in an unstable and chaotic flow of difficult study. Therefore, comparison with experiments will be here limited to the case of positive corona.

In order to match the experimental set-up used by Elagin et al., the top boundary (upper plate) in our modeling configuration (figure 2) has been suppressed. Therefore, excluding the lower plate and the wire, where a non-slipping condition is imposed, the rest of boundaries are treated as open boundaries, where pressure is assumed to be equal to the atmospheric pressure. However, these modifications do not affect the validity of the electrohydrodynamic force density previously obtained.

Figure 11 shows the numerical simulation of the flow pattern corresponding to the same experimental conditions as in one of the two experiments reported by Elagin et al., using a 11 cm long corona wire of radius 50 μm, and for an applied voltage of 13.5 kV. The general structure of the ionic wind velocity distribution matches closely the observations of Elagin et al., with an acceleration zone near the wire, a uniform flow zone in the central jet, and the formation of a stagnation zone when the jet collides with the plane. Then, the ionic wind jet flows sideways along the plate in opposite directions with a high velocity. A quantitative comparison between modeling and simulation is shown in Table 1, where the maximum the ion wind velocity is given for two different sets of electrical and geometrical parameters.

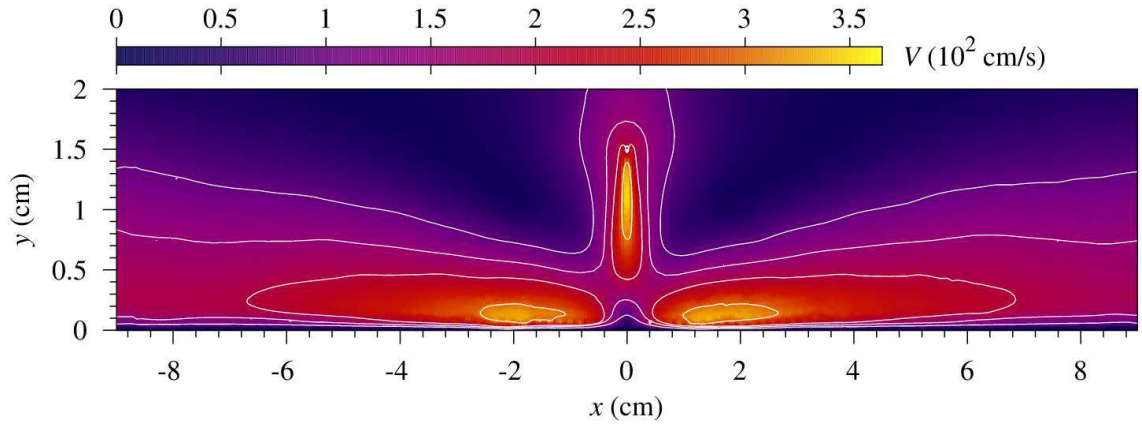

Figure 11. 2D-spatial distribution of the gas velocity magnitude corresponding to a positive corona discharge between a wire and a plate in an open channel. Streamlines are drawn as white solid lines. Wire radius: r_0 = 50 µm, wire length: w = 11 cm, wire-plate distance: d = 1.5 cm, applied voltage: ϕ = +13.5 kV, current intensity: I = 230 µA.

Table 1. Maximum ion wind velocity magnitude in wire-plate positive corona discharge for a wire of radius r_0 = 50 µm and length w = 11 cm. Comparison between numerical modeling and experiments.

			V_{max} (m/s)	
d (cm)	ϕ (kV)	I (µA)	numerical	experimental [4]
1.5	13.5	230	3.65	3.5
4	26	110	2.74	2.75

3.2 Parametric Study

In this section, the influence of different parameters on the electric wind velocity induced by the corona discharge will be investigated, both in the positive and in the negative polarity. For simplicity, the gas velocities will be only shown along the axis of symmetry. Three different parameters will be here considered: the applied voltage, the wire radius and the inter-electrode separation.

Effect of the applied voltage

Figure 12 shows the electric wind velocity along the y-axis corresponding to a positive (figure 12a) and a negative (figure 12b) corona discharge for three different values of the applied voltage: ±7 kV, ±9 kV, and ±11kV. The current intensities per unit of length corresponding to these voltages are, in the positive corona, 15.8 µA/cm, 47.4 µA/cm and 91.1 µA/cm, respectively, and, in the negative corona, −19.7 µA/cm, −59.3 µA/cm and −113.9 µA/cm, respectively.

As stated by (34), the raise of the applied voltage and, therefore, of the corona current intensity, implies an augmentation of the EHD force. Thus, an increase of the fluid velocity may be expected, as confirmed by the results presented in figure 12.

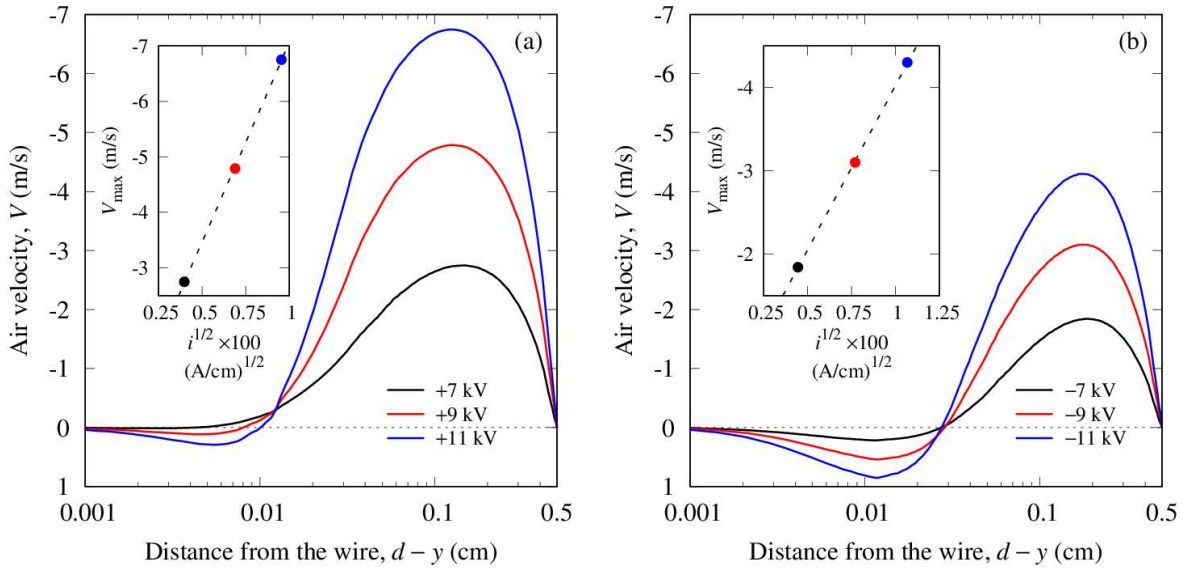

Figure 12. Gas velocity magnitude along the axis of symmetry (x = 0) in (a) positive corona and (b) negative corona, for three different values of the applied voltage: $\phi = \pm 7$, ± 9 and ± 11 kV. Wire radius: $r_0 = 100$ µm, inter-electrode separation: $d = 5$ mm.

In the positive corona (figure 12a), the flow velocity increases very rapidly beyond 100 µm from the wire: the higher the applied voltage, the faster the velocity gradient. However, in the vicinity of the wire, the velocity of the recirculating vortices also increases with the applied voltage. This augmentation is due to the shear with the adjacent mainstream flow, whose velocity has grown more rapidly with voltage. As previously said, in the positive corona, these vortices have mainly a hydrodynamic origin. This is confirmed by the fact that the length of the recirculating region increases as Reynolds number, Re, increases [40] (Re = Ud/ν, where U is the main stream flow velocity, d is the wire diameter and ν is the kinematic viscosity). At lower voltages, the recirculating flow tends to disappear.

In contrast, in the negative polarity, the air velocity is directed towards the wire along the first 300 µm, and towards the plate in the rest of the space. The velocity in the corona plasma region increases faster with the applied voltage than the drift region: the ratio of the maximum velocities in the plasma region and in the drift region is about 11% at −7 kV, and increases up to 21% at −9 kV. Finally, contrary to the positive corona, the coordinate at which the fluid velocity changes its sign is rather insensitive to the applied voltage, due to the active role played by the electric force in sustaining the vortices.

Different published data suggest an almost linear dependence of the averaged wind velocity with the square root of the discharge current [9, 41]. These observations are coincident with the results obtained from the present model since, as shown in the insets of figure 12, the maximum velocity scales as the square root of the current intensity, both in the positive and in the negative corona.

Effect of the wire radius

The effect of varying the wire radius on the EHD velocity is illustrated in figure 13 for an applied voltage of ±7 kV and an inter-electrode separation of 0.5 cm. Three values of the wire radius have been considered: 50 µm, 100 µm, and 150 µm.

According to Peek's law [35], the radius of the corona wire affects both the electric field on the cathode, $E_0 \approx 29.8 \times (1 + 0.301/r_0^{1/2})$ kV/cm, where r_0 is in cm, and the critical voltage for the onset of corona discharge, $\phi_c \approx E_0 r_0 \ln(2d/r_0)$. Decreasing the radius of the corona wire lowers the corona

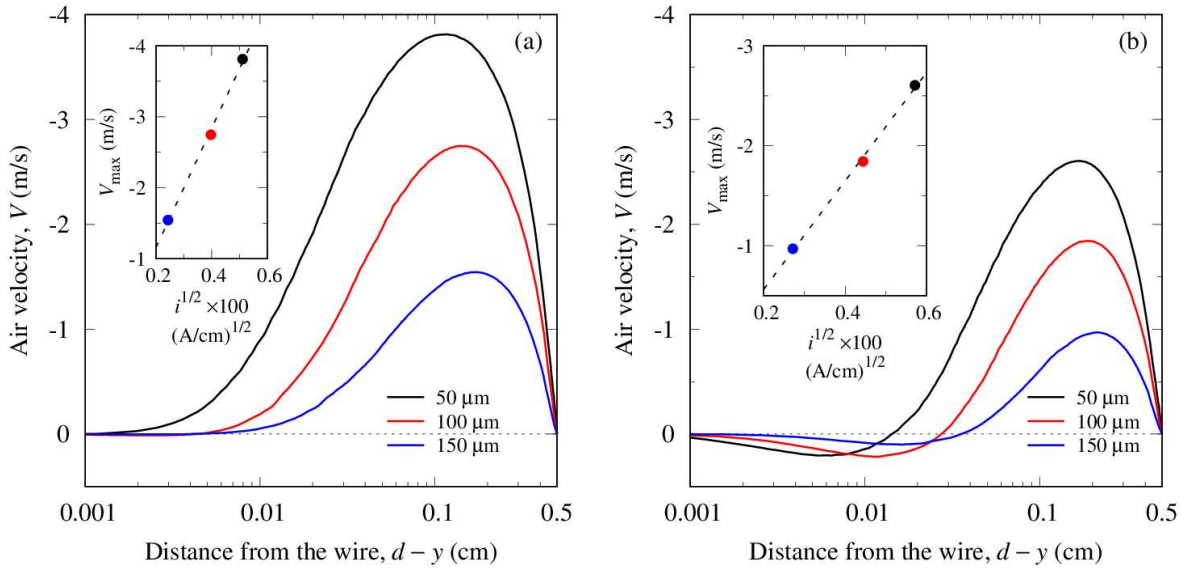

Figure 13. Gas velocity magnitude along the axis of symmetry (x = 0) in (a) positive corona, ϕ = 7 kV, and (b) negative corona, ϕ = −7 kV, for three different values of the wire radius: r_0 = 50 µm, 100 µm and 150 µm. Inter-electrode separation: d = 5 mm.

onset voltage and more current will flow for the same applied voltage. In particular, the corona currents per unit of length corresponding to the radii mentioned above are, for the positive polarity, 26.1 µA/cm, 15.8 µA/cm and 5.89 µA/cm, respectively, and, for the negative polarity, −32.7 µA/cm, −19.7 µA/cm and −7.36 µA/cm, respectively. Consequently, the smaller the wire radius, the higher the current intensity, the stronger the EHD force, and the faster the gas velocity. This correlation is readily observed on the results presented in figure 13: the air velocity in the drift region more than doubles when the radius is reduced from 150 µm to 50 µm, both in the positive and in the negative corona. Moreover, as in the previous case, the peak values of the flow velocity increases linearly with the square root of the current intensity (see insets in figure 13).

The variation of the wire radius also affects the flow velocity in the close vicinity of the wire. Since Reynolds number is proportional to the diameter of the wire, increasing the wire radius favors a longer recirculation region below the wire. In the positive corona (figure 13a), for the chosen applied voltage, the recirculation region is very weak, but this effect can be appreciate in the fact that the gas velocity directed towards the plate starts growing at a longer distance from the wire surface when the radius of the wire is increased.

In the negative corona, an additional factor comes into play. According to (19), the outer boundary of the ionization layer is located around $r_L = r_0 E_0 / E_L$, where E_L is the electric field for which the ionization and attachment coefficients become equal. Thus, the extent of the ionization region, $r_0(E_0 / E_L - 1)$, is enlarged when the radius of the corona wire becomes thicker and, correspondingly, there is an increase of the area where the electric force and the air motion is directed towards the wire (see figure 13b). The maximum fluid velocities in this region are similar for 50 µm and 100 µm, but larger than for 150 µm.

Effect of the inter-electrode separation

Figure 14 shows the effect of increasing the inter-electrode gap on the air velocity along the y-axis. Three values of the inter-electrode separations (5 mm, 7.5 mm and 1 cm) have been considered, for an applied voltage of ±7 kV and wire radius of 100 µm.

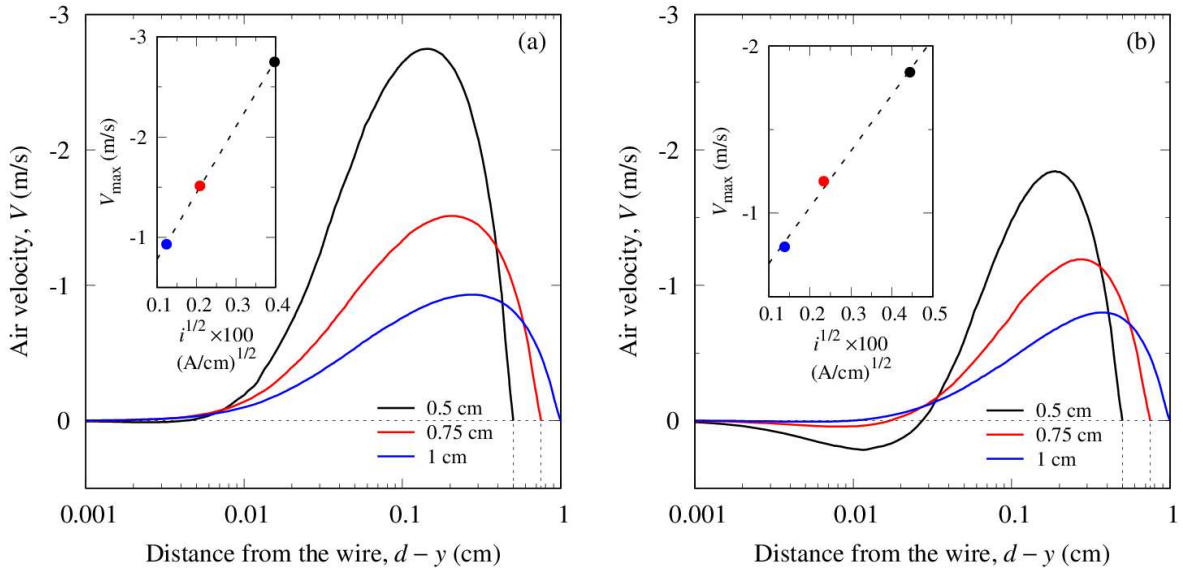

Figure 14. Gas velocity magnitude along the axis of symmetry (x = 0) in (a) positive corona, ϕ = 7 kV, and (b) negative corona, ϕ = −7 kV, for three different values of the inter-electrode separation: d = 0.5, 0.75 and 1 cm. Wire radius: r_0 = 100 μm.

As shown in the previous section, the critical voltage for the onset of corona discharge, $\phi_c \approx E_0 r_0 \ln(2d/r_0)$, is also affected by the electrode separation. As the distance between the wire and the plate is augmented, the corona onset voltage increases and, therefore, less current will flow for the same applied voltage. In the present case, the corona currents per unit of length corresponding to the inter-electrode gaps mentioned above are, for the positive corona, 15.8 μA/cm, 4.36 μA/cm and 1.53 μ A/cm, respectively, and, for the negative corona, −19.7 μA/cm, −5.45 μA/cm and −1.92 μA/cm, respectively. The reduction of current intensity means a lower EHD force and a decrease of the flow intensity in the drift region, which can be easily appreciated in figure 14. In the positive corona, the fluid velocity in the drift region decreases by nearly a factor 3 when the inter-electrode gap is doubled. In the negative corona, the corresponding reduction is of about a factor of 2. In both polarities, the point where the gas velocity reaches its maximum value moves away from the wire as the electrode separation is increased. As in the previous cases, the maximum flow velocity scales as the square root of the current intensity (see insets in figure 14).

In the negative corona, the secondary vortices beneath the wire are importantly affected by the separation of the electrodes, though according to Peek's law [35], the electric field on the wire surface is unaffected by the distance between the electrodes. However, since the current intensity decreases when the inter-electrode separation is raised, the density of electrons and ions in the ionization region must lower, and correspondingly the EHD force directed towards the wire. This fact, added to the lower velocity of the main stream flow around the wire, which favors a shorter recirculation region, leads to an important reduction of the extension and intensity of the velocity in this region. Therefore, as shown in figure 14b, the recirculation zone is progressively reduced and becomes negligible for an inter-electrode distance of 1cm.

4. Conclusions

A simplified formulation of the positive and negative corona discharge in air has been proposed to compute the gas flow generated by the EHD force. The approach assumes that the discharge gap is divided in two zones: the corona plasma region and the ion drift region. The first zone is a thin layer close to the corona electrode where ionization and electron attachment take place. The second zone corresponds to the rest of inter-electrode space, where ions with the same polarity as that of the corona

electrode carry the electric current. Semi-analytical expressions for the electric field and the current densities of electrons, positive ions and negative ions are obtained from the resolution of Gauss's law coupled with the continuity equations of charged particles. These approximated solutions can be evaluated with a minimal computational cost, which makes them interesting for the analysis and optimization of devices that employ corona discharge in different technological applications. Here, they have been used to obtain the expression of the EHD force responsible for the gas flow, which has been inserted in Navier-Stokes equations in order to compute the flow distribution.

The results of the simulation have shown that the structure of the plasma region of the corona discharge has a significant effect on the EHD gas flow. In the positive corona, the negative space charge is confined to a layer of negligible extent around the corona wire. Therefore, the electric force is directed towards the plate in the whole inter-electrode gap. In spite of this, two tiny vortices are observed beneath the wire, with recirculation velocities opposite to those in the adjacent large roll. These vortices have a hydrodynamic origin, since they are produced by the downwards air flow coming from above the wire. However, the electric force tends to damps down these vortices. In contrast, in the negative corona, the EHD force is directed towards the wire in the inner part of the plasma region, where ionization prevails over attachment and positive ions accumulate. Therefore, the electrical force helps to sustain the vortices generated underneath the wire. As a consequence, the effective length along which the fluid is accelerated towards the plate is reduced, precisely in the region where the electric force is more intense. Thus, the electric wind velocity observed in the negative corona is smaller than in the positive corona, even though the negative corona current is higher that the positive corona current at a given voltage. The simulation results have been compared with experimental measurements for the case of a positive corona, and a good agreement has been found.

The intensity of the electric wind is affected by the applied voltage, the wire radius and the inter-electrode separation but, in all cases, the maximum wind speed in the drift region scales as the square root of the current intensity, as reported in experimental observations. In particular, at a fixed voltage, reducing the wire radius and the inter-electrode distance leads to a faster EHD flow velocity. The secondary vortices located beneath the wire are also affected by these parameters, especially by the inter-electrode separation: they progressively die down when the gap between electrodes is increased.

Acknowledgments

This research has been funded by the Spanish Government Agency 'Ministerio de Economía y Competitividad' under contract no. FIS2014-54539-P.

References

[1] Cobine J D (1958) *Gaseous Conductors: Theory and Engineering Applications* (New York: Dover)

[2] Moreau E (2007) Airflow control by non-thermal plasma actuators *J. Phys. D: Appl. Phys.* **40** 605–636

[3] Molki M and Damronglerd P (2006) Electrohydrodynamic enhancement of heat transfer for developing air flow in square ducts *Heat Transfer Eng*. **27** 35–45

[4] Elagin I A, Yakovlev V V, Ashikhmin I A, and Stishkov Yu K (2016) Experimental Investigation of Cooling of a Plate by Ionic Wind from a Corona-Forming Wire Electrode *Technical Physics* **61** 1214–1219

[5] Zhao L and Adamiak K (2016) EHD flow produced by electric corona discharge in gases: From fundamental studies to applications (a review) *Part. Sci. Technol.* **34** 63-71

[6] Birhane Y T, Lin S-C and Lai F C (2017) Flow characteristics of a two-stage EHD gas pump in a circular pipe *IEEE Trans. Ind. Appl.* **53** 2461-2470

[7] Léger L, Moreau E and Touchard G (2002) Effect of a DC corona electrical discharge on the airflow along a flat plate *IEEE Trans. Ind. Appl.* **38** 1478- 1485

[8] Bastien F (1987) Acoustics and gas discharges: application to loudspeakers *J. Phys. D: Appl. Phys.* **20** 1547–1557

[9] Robinson M (1961) Movement of air in the electric wind of the corona discharge *AIEE Transactions* **80** 143-150

[10] Béquin Ph, Castor K and Scholten J (2003) Electric wind characterisation in negative point-to-plane corona discharges in air *Eur. Phys. J. AP* **22** 41-49

[11] Lacoste D A, Pai D and Laux C (2004) Ion wind effect in a positive dc corona discharge in atmospheric pressure air *42nd AIAA Aerospace Sciences Meeting and Exhibit (Reno, Nevada, 5-8 January 2004)*

[12] Zhao L and Adamiak K (2009) Effects of EHD and external airflows on electric corona discharge in point-plane/mesh configurations *IEEE Trans. Ind. Appl.* **45** 16-21

[13] Zhao L and Adamiak K (2013) Numerical simulation of the effect of EHD flow on corona discharge in compressed air *IEEE Trans. Ind. Appl.***49** 298-304

[14] Ahmedou S O and Havet M (2009) Effect of process parameters on the EHD airflow *J. Electrostat.* **67** 222–227

[15] Seimandi P, Dufour G and Rogier F (2009) An asymptotic model for steady wire-to-wire corona discharges *Math Comput Model* **50** 574-583

[16] Cagnoni D, Agostini F, Christen T, Parolini N, Stevanovic I and de Falco C (2013) Multiphysics simulation of corona discharge induced ionic wind *J. Appl. Phys.* **114** 233301

[17] Chen S, Nobelen J C P Y and Nijdam S (2017) A self-consistent model of ionic wind generation by negative corona discharges in air with experimental validation *Plasma Sources Sci. Technol.* **26** 095005

[18] Chen J H and Davidson J H (2003) Model of the negative DC corona plasma: comparison to the positive dc corona plasma *Plasma Chem. Plasma Process.* **23** 83-102

[19] Zhang J and Adamiak K (2007) A multi-species DC stationary model for negative corona discharge in oxygen; point-plane configuration *J. Electrostat.* **65** 459–464

[20] Yanallah K and Pontiga F (2012) A semi-analytical stationary model of a point-to-plane corona discharge *Plasma Sources Sci. Technol*. **21** 045007

[21] Yanallah K, Pontiga F and Chen J H (2013) A semi-analytical study of positive corona discharge in wire–plane electrode configuration *J. Phys. D: Appl. Phys.***46** 345202

[22] Yanallah K, Pontiga F, Meslem Y and Castellanos A (2012) An analytical approach to wire-to-cylinder corona discharge *J. Electrostat.* **70** 374-383

[23] Yanallah K, Pontiga F, Bouazza M R and Chen J H (2017) The effect of the electric wind on the spatial distribution of chemical species in the positive corona discharge *J. Phys. D: Appl. Phys* **50** 335203

[24] Vann Bush P and Snyder T R (1987) Laboratory analyses of corona discharges *J. Electrostat*. **19** 83–99

[25] Chang J S, Lawless P A and Yamamoto T (1991) Corona discharge processes *IEEE Trans. Plasma Sci.* **19** 1152–1166

[26] Morrow R (1985) Theory of negative corona in oxygen *Phys. Rev. A* **32** 1799–1809

[27] Kulikovsky A A (1997) The mechanism of positive streamer acceleration and expansion in air in a strong external field *J. Phys. D: Appl. Phys.* **30** 1515–1522

[28] Morse P M and Feshbach H (1953) *Methods of Theoretical Physics* (New York: McGraw-Hill)

[29] Spiegel M R, Lipschutz S and Liu J (1998) *Mathematical Handbook of Formulas and Tables* (New York: McGraw-Hill).

[30] Sigmond R S (1986) The unipolar corona space charge problem, *J. Electrostat.* **18** 249–272

[31] Hagelaar G J M BOLSIG+: Electron Boltzman Equation Solver [online] http://www.bolsig.laplace.univ-tlse.fr (accessed July 2015)

[32] Hagelaar G J M and Pitchford L C (2005) Solving the Boltzmann equation to obtain electron transport coefficients and rate coefficients for fluid models *Plasma Sources Sci. Technol.* **14** 722-33

[33] Warburg E (1927) *Characteristik des spitzenstromes, Handbuch der Physik* (Berlin: Springer).

[34] Zebboudj Y 2000 Measurements of current and electric field distributions beneath a positive DC wire-to-plane corona using a linear biased probe *IEE Proc.-Sci. Meas. Technol.* **147** 74–80

[35] Peek F W (1929) *Dielectric Phenomena in High Voltage Engineering* (New York: McGraw-Hill).

[36] Boeuf J P and Pitchford L C (2005) Electrohydrodynamic force and aerodynamic flow acceleration in surface dielectric barrier discharge *J. Appl. Phys.* **97** 103307

[37] Versteeg H K and Malalasekera W 2007 An Introduction to Computational Fluid Dynamics. The Finite Volume Method (Harlow: Pearson Education)

[38] ANSYS® Academic Research, Release 15.0 http://www.ansys.com/

[39] Deutsch W (1933) Über die Dichteverteilung unipolarer Ionenströme *Ann. Phys*. **408** 588–612.

[40] Guyon E, Hulin J-P, Petit L and Mitescu C D (2015) *Physical Hydrodynamics* (New York: Oxford University Press).

[41] Kozlov B A and Solovyov V I (2007) Electric wind in electrode systems with corona points *Technical Physics* **52** 892–897